Int. J. Electrochem. Sci., 7 **(2012)** 7152 - 7164

International Journal of
ELECTROCHEMICAL
SCIENCE
www.electrochemsci.org

Synthesis and Electrochemical Characteristics of an Orthorhombic $LiMnO_2$ Cathode Material Modified With Poly(Vinyl-Pyrrolidone) for Lithium Ion Batteries

Cong Liu, Junmin Nan[*]*, Xiaoxi Zuo, Xin Xiao, Dong Shu*

School of Chemistry and Environment, South China Normal University, Guangzhou 510006, P.R. China
[*]E-mail: jmnan@scnu.edu.cn

Received: 5 May 2012 / *Accepted:* 13 July 2012 / *Published:* 1 August 2012

The orthorhombic $LiMnO_2$ (o-$LiMnO_2$) cathode materials modified with poly(vinyl-pyrrolidone) (PVP) for lithium ion batteries are synthesized by using a solid-state reaction and subsequently the hydrothermal method. The modified materials are characterized using X-ray diffraction (XRD), fourier transform infrared spectroscopy (FTIR), thermogravimetric analysis (TGA), differential scanning calorimetry (DSC), scanning electron microscope (SEM), and electrochemical techniques. It is shown that the bare o-$LiMnO_2$ sample with high purity is synthesized at 750 °C under nitrogen atmosphere using Mn_2O_3 and $LiOH{\cdot}H_2O$ as precursors, and it has a higher discharge capacity than other samples containing impurity phases. The poly(vinylpyrrolidone) (PVP) is modified into the bare o-$LiMnO_2$ particles by the hydrothermal method at 140 °C for 4 days. The C=O and C–N bonds in PVP bond with the Mn atoms in the o-$LiMnO_2$; a partially modified PVP successfully intercalates into the lattice of o-$LiMnO_2$ and opens its interlayers. The highest specific capacity and most improved cycling property are obtained for PVP-o-$LiMnO_2$ with about 3.7 wt.% PVP. The enhancement of the cycling property of PVP-o-$LiMnO_2$ can be attributed to the protection of the spinel-like structure formed upon cycling by PVP.

Keywords: orthorhombic $LiMnO_2$; poly(vinyl-pyrrolidone); synthesis; modification; electrochemical performance.

1. INTRODUCTION

Lithium-manganese-oxide compounds such as $LiMn_2O_4$ [1,2], $Li_4Mn_5O_{12}$ [3], and $LiMnO_2$ [1,4-22] are candidate materials to replace the commercial $LiCoO_2$ cathode in lithium-ion secondary batteries because of their low-cost and environmental friendliness. Spinel $LiMn_2O_4$, unfortunately, delivers a lower discharge capacity (110–120 mAh g^{-1}) than $LiCoO_2$ (140–150 mAh g^{-1}). It also faces

structural instability due to Jahn-Teller (J-T) distortion [1,2] and severe capacity fading problems due to the dissolution of manganese on cycling, especially at elevated temperatures (> 50 °C). Orthorhombic $LiMnO_2$ material, which has a zigzag β-$NaMnO_2$ layered structure (space group Pmnm), has attracted considerable attention due to its theoretical capacity (285 mAh g^{-1}) being nearly twice as large as that of spinel $LiMn_2O_4$ material (148 mAh g^{-1}) for the same Mn^{4+}/Mn^{3+} redox couple over a wide voltage range .

The layered $LiMnO_2$ exists as monoclinic and orthorhombic polymorphs (hereafter referred to as m-$LiMnO_2$ and o-$LiMnO_2$, respectively). The o-$LiMnO_2$ polymorphs are generally considered to be more stable than the m-$LiMnO_2$ polymorphs [4-5]. The reported methods for the synthesis of o-$LiMnO_2$ are based on not only high-temperature solid-state reactions [6-10], but also on wet chemical processes such as ion exchange [11], hydrothermal [12,13], sol-gel [14,15], and reverse-microemulsion [16] methods. Although the microstructure, morphology and properties of o-$LiMnO_2$ materials could be easily adjusted by the wet chemical processes due to their lower synthesizing temperatures and highly variable reaction parameters, the solid-state reaction processes are still considered to be the preferential synthesis technique for ease of mass production.

The capacity losses caused by charge-discharge processes plague the commercial use of o-$LiMnO_2$ materials. These losses are usually attributed to the destabilization of the layered structure of o-$LiMnO_2$ materials upon Li^+ deintercalation- intercalation [6,7]. In order to minimize the structural transformation and performance decay of o-$LiMnO_2$ materials during charge discharge processes, a small quantity of metal ions such as Co [17], Ni [18], Al [19], Mg [20], Fe [21], or In [22] is usually used to partially substitute the Mn, a method commonly performed in the synthesis of other Li-Mn-O compounds. It has been reported that o-$LiMnO_2$ changes to a phase that has a spinel-like structure during cycling. The dissolution of Mn is again the cause of poor cycling performance and leads to defective spinels [1,6,7,9]. The ability of o-$LiMnO_2$ materials to experience surface modifications by inorganic or polymeric materials is based on the inherent properties of the surface species. Li et al. [23] reviewed the modification performances of coating the cathode materials of lithium ion batteries. They pointed out that when the surface of the cathode materials, including $LiCoO_2$, $LiNiO_2$, $LiMn_2O_4$ and $LiMnO_2$, was coated with oxides such as MgO, Al_2O_3, SiO_2, TiO_2, ZnO, SnO_2, ZrO_2, and $Li_2O{\cdot}2B_2O_3$-glass, the coatings prevented direct contact with the electrolyte solution, suppressed phase transition, improved structural stability, and decreased the disorder of cations in crystal sites. It was also found that CoO [24] and Al_2O_3 [25] were the most promising modifiers of $LiMnO_2$. Besides investigation the modification capabilities of inorganic species, Amatucci et al. [26] used acetylacetone as a complex agent to modify $Li_{1+x}Mn_{2-x}O_4$ spinels. After annealing at 800 °C as post-treatment, they found the irreversible capacity loss decreased after several weeks of storage at 55 °C due to the formation of a protective barrier layer between the liquid electrolyte and the spinel surface. Pasquier et al. [27] obtained poly(pyrrole) (PPy) coated $Li_{1.05}Mn_{1.95}O_4$ by reacting $Li_{1.05}Mn_{1.95}O_4$ and pyrrole in a paratoluene sulfonic acid_aqueous solution and found that $Li_{1.05}Mn_{1.95}O_4$-PPy with low PPy content had a higher capacity and an improved cycling lifetime at room temperature. This was because the reaction between pyrrole and $LiMn_2O_4$ in an acidic medium caused a surface modification of the spinel that partially prevented the cathode from further capacity fading.

We synthesized pure o-$LiMnO_2$ cathode material by a solid-state reaction process using Mn_2O_3 and $LiOH{\cdot}H_2O$ as precursors. We also used poly(vinylpyrrolidone) (PVP) as a modification agent because it is a high molecular weight polymer that is water-soluble and nontoxic, has high mechanical stability and good heat-resistant capability, and can form cooperation complexes with many inorganic compounds due to the carbonyl and amide groups contained in its framework [28]. PVP was introduced to enhance the pure o-$LiMnO_2$ through a hydrothermal method. In this paper, the synthesis and the electrochemical properties of o-$LiMnO_2$ cathode materials modified with PVP (hereafter referred as PVP-o-$LiMnO_2$) are presented.

2. EXPERIMENTAL

2.1. Synthesis of o-$LiMnO_2$ and PVP-o-$LiMnO_2$

The o-$LiMnO_2$ compounds were synthesized using a solid-state reaction. The electrolytic MnO_2 (≥ 99.0%) was first heated at 800 °C in air for 10 h to obtain the Mn_2O_3 precursor. Then, a mixture of Mn_2O_3 and $LiOH{\cdot}H_2O$ (≥ 96.0%) in a stoichiometric molar ratio (Mn:Li =1:1.05) was grounded for 12 h by wet ball milling in an anhydrous ethanol solution to ensure intimate and homogeneous mixing. A little excess Li precursor was used to compensate for the Li loss from the heat-treatment [29]. Afterwards, the mixed precursors were heat-treated under nitrogen atmosphere for 24 h and subsequently cooled to room temperature to obtain the pure o-$LiMnO_2$.

A 1 g sample of PVP was dissolved in 20 ml distilled water and then mixed with 5 g pure o-$LiMnO_2$ particles under vigorous stirring for 6 h. The mixed polyblend was directly poured into Teflon-lined autoclaves and kept at 140 °C for 4 days. After the hydrothermal reaction, the black product was washed with distilled water and ethanol and subsequently dried at 100 °C for 8 h to obtain PVP-o-$LiMnO_2$ sample. Oxygen post-treatment was carried out by heating the PVP-o-$LiMnO_2$ particles at 100 °C for 4 h under oxygen atmosphere in a pipe furnace in order to activate the PVP modified on $LiMnO_2$ particles [30].

2.2. Characterization of o-$LiMnO_2$ and PVP- o-$LiMnO_2$

The powder X-ray diffraction (XRD 6000, Shimazu, Japan) using Cu Kα radiation was employed to identify the crystalline phase of the o-$LiMnO_2$ and PVP-o-$LiMnO_2$ samples. Fourier transform infrared (FTIR 17300, Perkin-Elmer, USA) absorption spectra were recorded with a resolution of 4 cm^{-1} and over a range of 400 – 4,000 cm^{-1} to identify characteristic groups in the samples. Thermogravimetric analysis (TGA) and differential scanning calorimetry (DSC) (Perkin-Elmer, USA) were carried out at atmosphere to measure the content of PVP on the o-$LiMnO_2$ particles. The particle morphologies of the bare o-$LiMnO_2$ and PVP-o-$LiMnO_2$ samples were observed with a scanning electron microscope (SEM, JSM 6380, Micron, USA).

The electrochemical performances of the as-synthesized bare o-$LiMnO_2$ and PVP-o-$LiMnO_2$ samples were evaluated with CR2032 coin cells, which were fabricated with a metallic lithium anode,

UP3085 polypropylene separator, and 1 mol L^{-1} $LiPF_6$ in 1:1 ethylene carbonate (EC) and diethyl carbonate (DEC) electrolyte in an argon filled glove box (MKSS1-0510-0107, Mikrouna, USA). The cathodes were prepared by mixing 75 wt.% PVP-o-$LiMnO_2$ (or o-$LiMnO_2$), 10 wt.% Super P carbon black, 5 wt.% graphite, and 10 wt.% polyvinylidene fluoride (PVDF) binder, rolling the mixture into thin sheets, and punching circular electrodes of 1.13 cm^2 area that typically had 15 mg active material. The cells thus fabricated were cycled galvanostatically in the range of 2.0–4.2 V at a current density of 0.13 $mA \cdot cm^{-2}$ (0.5 C rate) at room temperature with a CT2001A battery test instrument (Wuhan Kingnuo, China).

3. RESULTS AND DISCUSSION

3.1 Microstructure and morphology of o-$LiMnO_2$ and PVP-o-$LiMnO_2$

The XRD patterns of the o-$LiMnO_2$ samples synthesized at 650 – 850 °C for 24 h under nitrogen atmosphere are shown in Figure 1a. It can be seen that the peaks of the o-$LiMnO_2$ samples became prominent with increasing heat-treatment temperature, indicating the orthorhombic structure became well-ordered at higher temperatures. The diffraction peaks of the o-$LiMnO_2$ sample calcined at 750 °C were consistent with the standard values of JCPDS No. 35-0749, showing the pure o-$LiMnO_2$ phase was obtained. The other peaks corresponding to monoclinic Li_2MnO_3 and tetragonal $Li_2Mn_2O_4$ were observed at other temperatures. The impurities appeared at temperatures less than 750 °C were ascribed to the incomplete solid reaction, while the appearance of the $LiMn_2O_4$ phase at 800 °C and 850 °C were attributed to the phase transformation. This indicates that the Li-Mn-O compounds with a spinel rather than layered structure were easily formed if the calcining temperatures were not carried out properly. In the latter electrochemical experiments, it was also indicated that the pure o-$LiMnO_2$ sample discharged a higher capacity than the other samples and thus, the pure o-$LiMnO_2$ sample synthesized at 750 °C was selected to be modified by PVP.

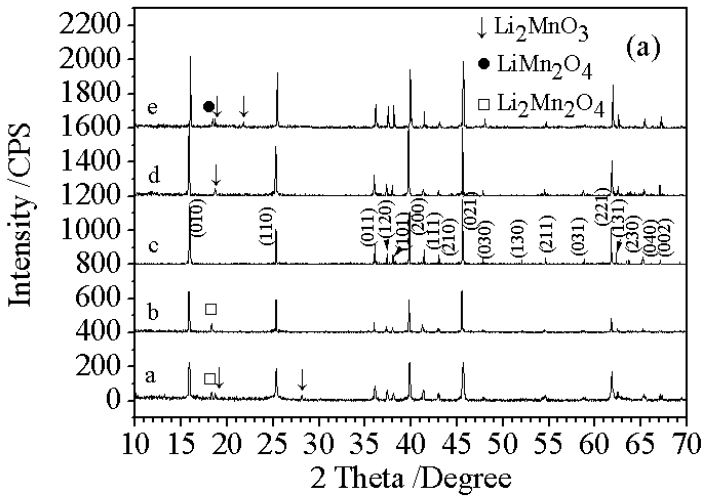

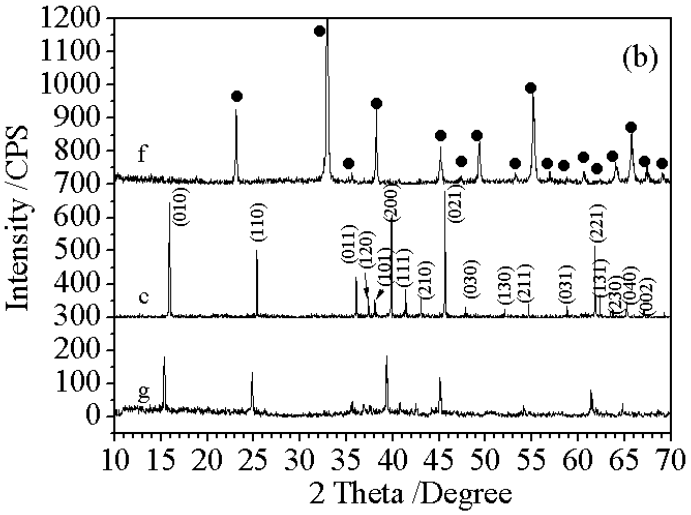

Figure 1. XRD spectra of o-$LiMnO_2$ synthesized at (a) 650 °C, (b) 700 °C, (c) 750 °C, (d) 800 °C and (e) 850 °C temperature for 24 h under nitrogen atmosphere; and of (f) Mn_2O_3 precursor and (g) PVP-o-$LiMnO_2$

The XRD patterns of the manganese oxide (Mn_2O_3) precursor, the bare o-$LiMnO_2$ sample, and the PVP-o-$LiMnO_2$ samples are shown in Figure 1b. The XRD spectrum of the Mn_2O_3 precursor indicates the presence of a pure Mn_2O_3 state, which played an important role in the synthesis of pure o-$LiMnO_2$. In comparison with the bare o-$LiMnO_2$, PVP-o-$LiMnO_2$ had lower diffraction peak intensities overall; the (030), (130) and (031) peaks even disappeared, indicating the coating of PVP on the bare o-$LiMnO_2$ surface and the increasing amorphosity in bare o-$LiMnO_2$ interlayer [30] had a significant effect. In addition, it can be seen that the diffraction peaks shifted to the lower angle side and can be ascribed to the increasing distance between the interlayers of o-$LiMnO_2$, confirming that the PVP was intercalated into the microstructure of o-$LiMnO_2$ and subsequently opened its interlayer.

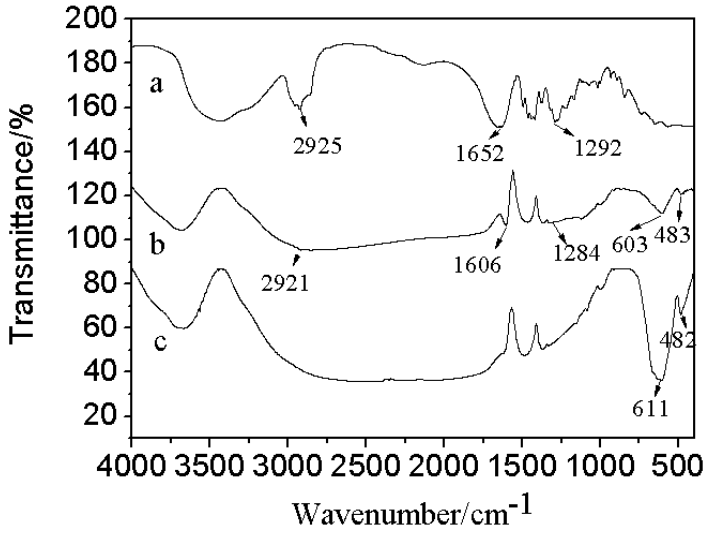

Figure 2. FTIR spectra of (a) PVP, (b) PVP-o-$LiMnO_2$, and (c) bare o-$LiMnO_2$

The FTIR spectra of the hybrid particles also clearly demonstrate the presence of PVP on bare o-$LiMnO_2$. Figure 2 shows the FTIR spectra of bare o-$LiMnO_2$, PVP-o-$LiMnO_2$ and pure PVP. The bare o-$LiMnO_2$ exhibited two main vibration peaks at 482 and 611 cm^{-1}, which correspond to the asymmetry and symmetry stretching modes (v_{as} and v_s) of Mn–O, respectively [27,31]. The FTIR spectrum of PVP- o-$LiMnO_2$ shows the characteristic peaks of PVP at 1284 and 2925 cm^{-1}, i.e. the v_s (C–N) stretching vibration and the C–H stretching vibration, confirming the presence of PVP. Additionally, the PVP peaks at 1652 and 1292 cm^{-1}, which correspond to the C=O stretching vibration and the v_s (C–N) stretching vibration of PVP, blue shifted to 1606 and 1284 cm^{-1}, along with the v_s (Mn–O) peak from 611 to 603 cm^{-1}, affirming that the C=O and C–N bonds of PVP bonded with the Mn atoms in o-$LiMnO_2$.

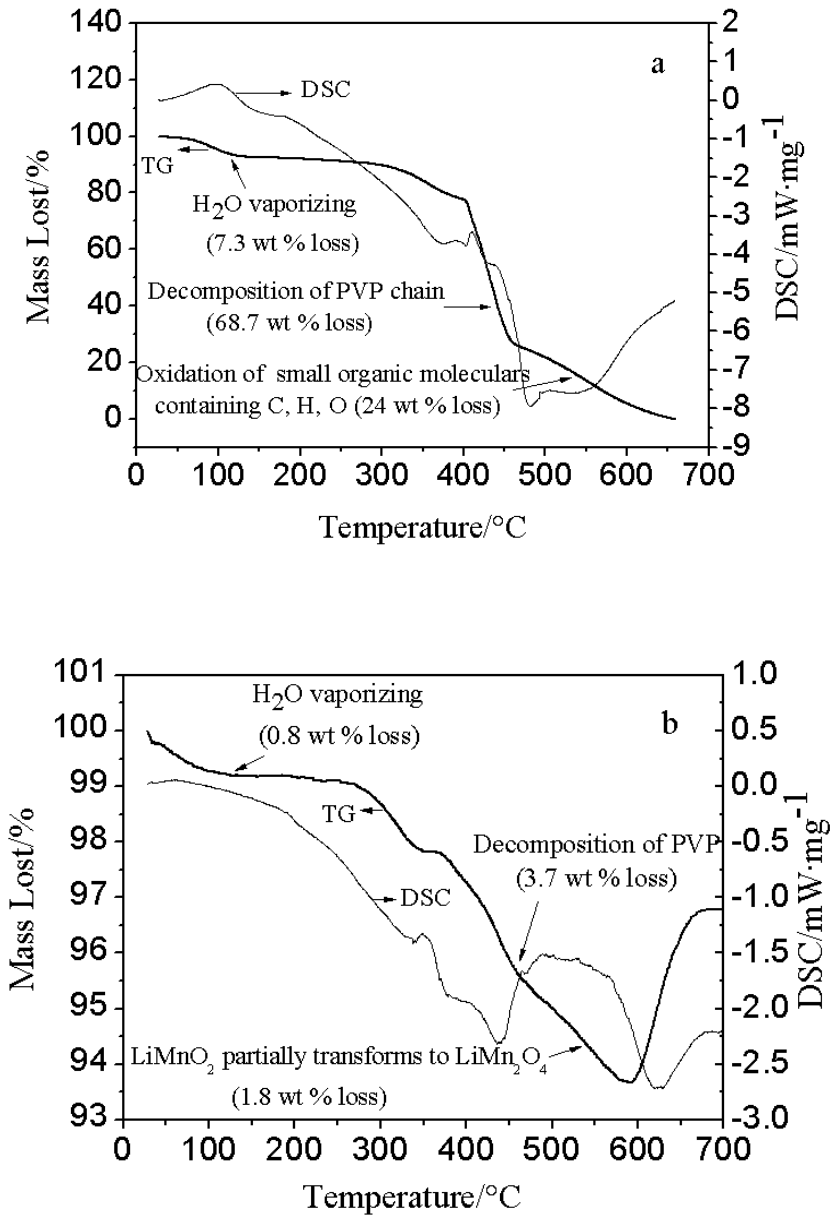

Figure 3. TG-DSC curves of (a) pure PVP and (b) PVP-o-$LiMnO_2$

The PVP and the PVP-o-$LiMnO_2$ hybrid particles were investigated by thermochemical methods. TG and DSC measurements were carried out at heating rates of 20 °C min^{-1} and 10 °C min^{-1}, respectively. The typical TG and DSC curves of PVP and PVP-o-$LiMnO_2$ are shown in Figure 3. The PVP curve (Figure 3a) showed a three-step weight loss in the temperature range of 27 – 650 °C. The first weight loss of around 7.3 wt.% in the temperature range of 40 – 140 °C is associated with the removal of absorbed water. The second weight loss of 68.7 wt.% in the 350 – 500 °C range (seen in the corresponding exotherm curve in the DSC) is associated with the decomposition of PVP chain. The third weight loss of 24 wt.% in the 500 – 650 °C range (seen also in the corresponding endotherm curve in the DSC) is associated with the oxidation of small organic molecules. The PVP- (o-$LiMnO_2$) curve (Figure 3b) also exhibited a three-step weight loss in the temperature range of 29 – 600 °C. The first weight loss around 0.8 wt.% in the temperature range of 29 – 120 °C is associated with the removal of absorbed water. The second weight loss of 3.7 wt.% in the 250 – 460 °C range (seen in the corresponding exotherm curve in DSC) is associated with the decomposition of PVP, in agreement with Figure 3a. The third weight loss of 1.8 wt.% in the 460 – 590 °C range (seen also in the corresponding endotherm curve in the DSC) is associated with the partial transformation of $LiMnO_2$ to $LiMn_2O_4$. From these curves, the content of PVP modified on bare o-$LiMnO_2$ was estimated to be about 3.7 wt.%.

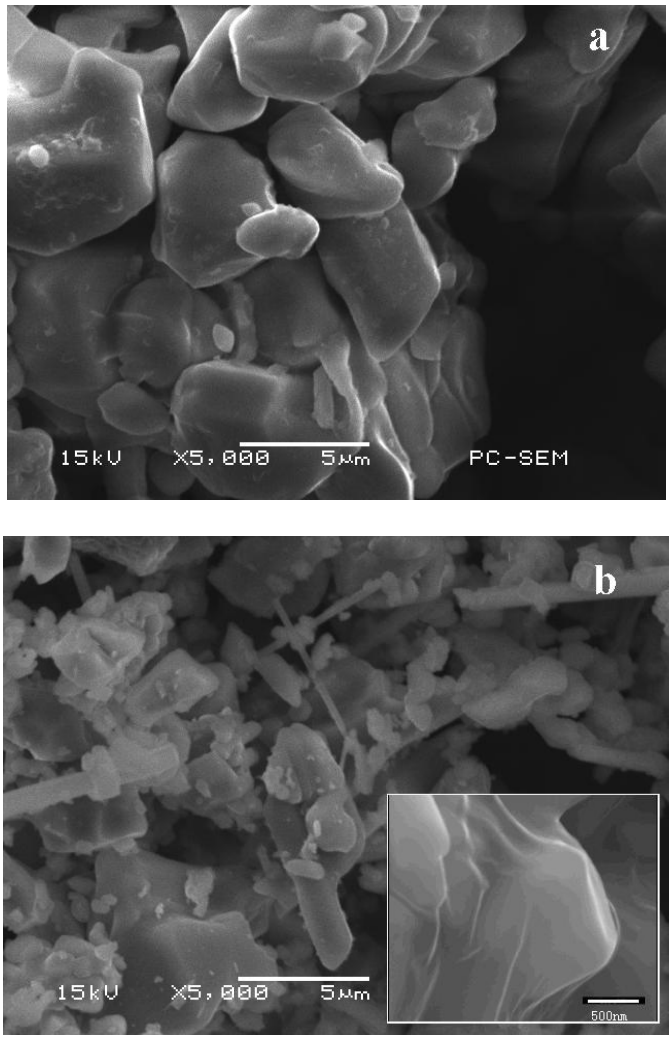

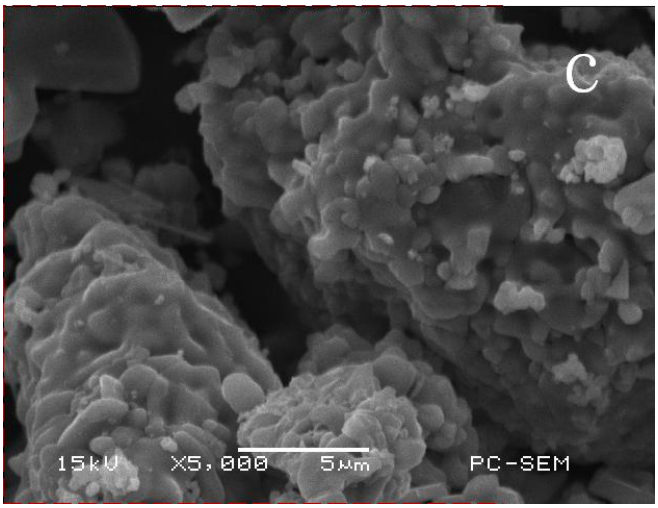

Figure 4. SEM micrographs of (a) bare o-$LiMnO_2$, (b) PVP-o-$LiMnO_2$, and (c) bare o-$LiMnO_2$ treated by the hydrothermal method

Figure 4 shows the SEM images of bare o-$LiMnO_2$ and PVP-o-$LiMnO_2$ particles. The bare o-$LiMnO_2$ particles treated by the hydrothermal method without PVP are also presented in Figure 4 to illustrate the effect of the treatment on the morphology of o-$LiMnO_2$. It can be seen that the particle morphology changed significantly under different hydrothermal conditions. Compared with the other two samples (Figure 4a and Figure 4c), small particles and some fiber or stick typed crystals appeared in the PVP-o-$LiMnO_2$ sample (Figure 4b), even though the recrystallization process occurring on the surface of the particles dramatically decreased when PVP was added to the hydrothermal solution. The coating of PVP is clearly seen on the particle surface in the higher-resolution inset of the image in Figure 4b. The PVP coating offered a layer between the o-$LiMnO_2$ particle and the surrounding electrolytic solution and subsequently affected the surface properties of o-$LiMnO_2$ particles in the charge-discharge process. Sapra et al. [32] and Liu et al. [33] observed that PVP might influence the Ostwald ripening kinetics, thereby causing the growth rate to decrease with increasing size of the particles. Hence, only PVP-o-$LiMnO_2$ particles within a narrow size distribution could be obtained, as observed here. Correspondingly, only the recrystallization of ions happened on the surface of o-$LiMnO_2$ particles when PVP was not used in the hydrothermal process.

3.2 Electrochemical characteristics of bare o-$LiMnO_2$ and PVP-o-$LiMnO_2$

Figure 5 shows the initial discharge capacities of o-$LiMnO_2$ synthesized at different temperatures. A charge-discharge current of 0.1 C (0.025 mA cm^{-2}) was used between 4.2–2.0 V. It is seen that the sample synthesized at 750 °C discharged at higher capacity than the other samples and gave the highest capacity (163 mAh g^{-1}) at the 18th cycle. As shown in Figure 1, since the sample synthesized at 750 °C had a pure o-$LiMnO_2$ phase, it can be concluded that the pure o-$LiMnO_2$ sample had a higher electrochemical capacity-storage capability than the samples with impurity phases.

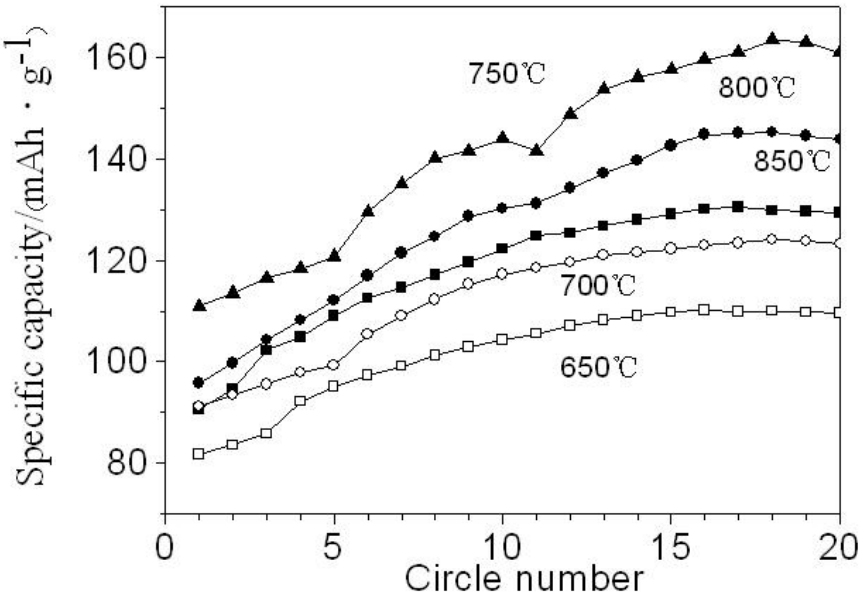

Figure 5. Curves of discharge capacity vs. cycle number for o-$LiMnO_2$ synthesized at different temperatures at 0.1 C (0.025 mA cm^{-2}) between 4.2–2.0 V

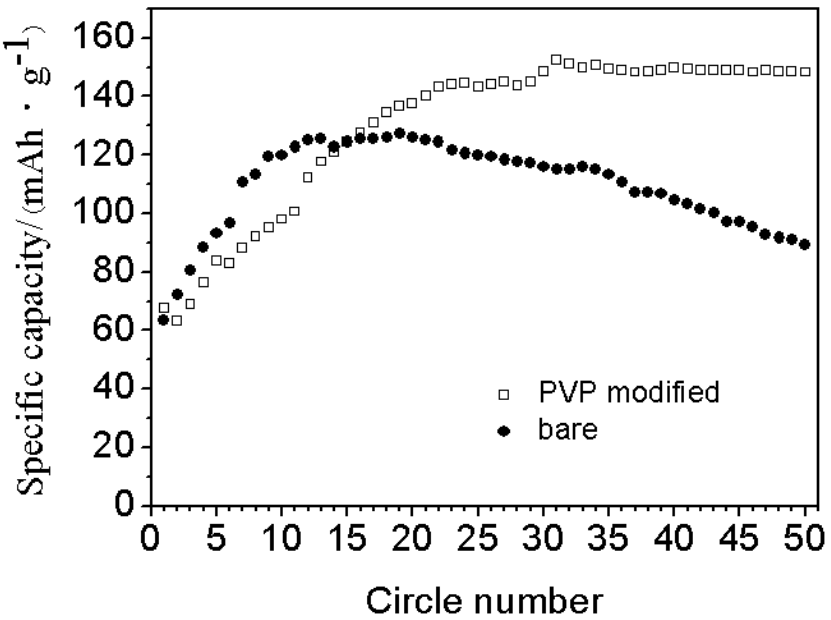

Figure 6. Curves of discharge capacity vs. cycle numbers for bare o-$LiMnO_2$ and PVP-o-$LiMnO_2$ charge- discharged at 0.5 C (0.13 mA cm^{-2}) between 4.2–2.0 V

Figure 6 shows the cycling curves of the as-synthesized bare o-$LiMnO_2$ and PVP-o-$LiMnO_2$ charge-discharged at 0.5 C (0.13 mA cm^{-2}) between 4.2–2.0 V. As seen in previous studies [9,10,23], there was low initial discharge capacity for the as-synthesized pure o-$LiMnO_2$ material (63 mAh g^{-1}). Its discharge capacity then increased and reached the highest value of 127 mAh g^{-1} after 19 cycles. The highest discharge capacity of 127 mAh g^{-1} was ~16% smaller than the highest discharge of PVP-o-

$LiMnO_2$ at 0.025 mA cm^{-2}, suggesting that the low conductivity of o-$LiMnO_2$ was a vital factor to its high electrochemical performance [1,23]. After reaching its maximum value, the discharge capacity of the as-synthesized pure o-$LiMnO_2$ material decreased to 89 mAh g^{-1} after 50 cycles. The low initial discharge capacity of the o-$LiMnO_2$ synthesized by the high-temperature solid-state reaction can be attributed to the intrinsic properties of pure o-$LiMnO_2$.

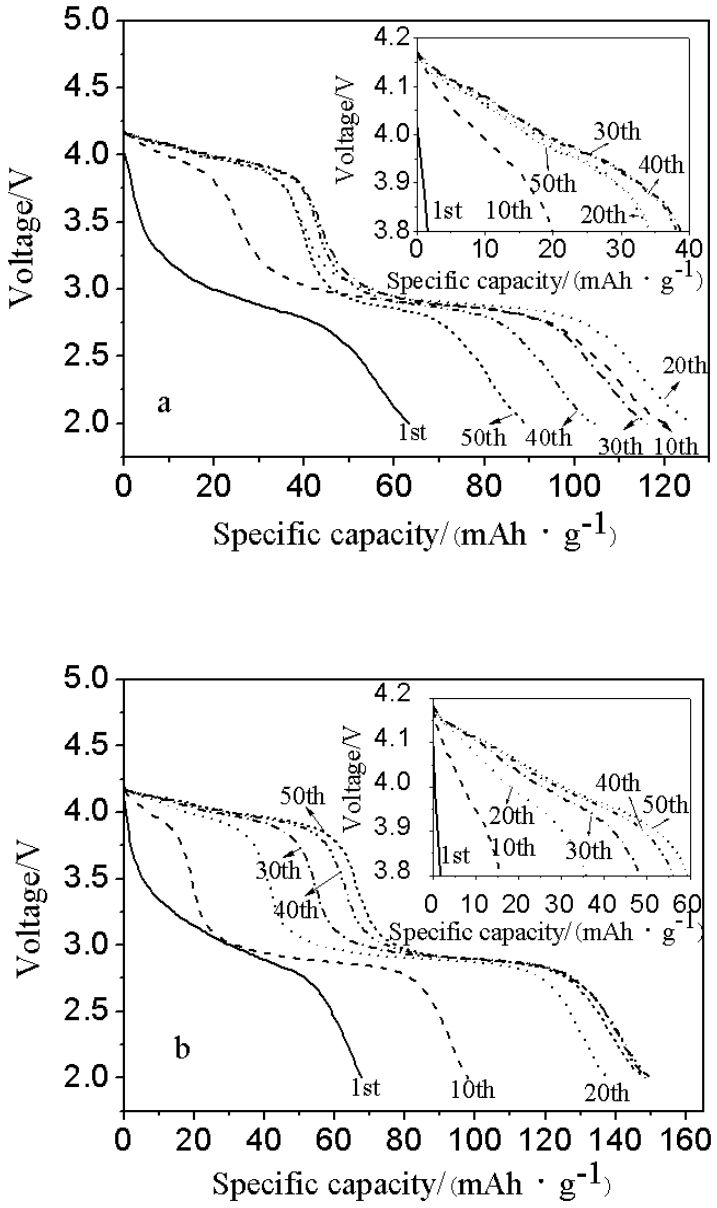

Figure 7. Discharge curves of (a) bare o-$LiMnO_2$ and (b) PVP-o-$LiMnO_2$ at 0.5 C (0.13 mA cm^{-2}) between 4.2 – 2.0 V

The subsequent increase in discharge capacity is due to the transformation, upon cycling, of o-$LiMnO_2$ to a phase with a spinel-like structure. Although the initial discharge capacity of PVP-o-$LiMnO_2$ was similar to that of bare o-$LiMnO_2$, PVP-o-$LiMnO_2$ discharged at a higher capacity of 152 mAh g^{-1} after 31 cycles and then remained at around 150 mAh g^{-1} during subsequent cycles. The

similar initial capacities of PVP-o-$LiMnO_2$ and of bare o-$LiMnO_2$ indicated that the hydrothermal treatment had no visible effects on the intrinsic properties of pure o-$LiMnO_2$. However, comparing the capacity losses of the bare o-$LiMnO_2$ (30%) and of PVP-o-$LiMnO_2$ (2.6% after 50 cycles), it can be clearly observed that the cyclability of PVP-o-$LiMnO_2$ was enhanced after the modification of PVP. From the discharge curves shown in Figure 7, only one voltage plateau around 2.9 V was observed for the first cycle. Around 4 V, additional voltage plateaus appeared; from Figure 6, it was observed that at this voltage, the discharge capacities simultaneously increased as the number of cycles rose to 20. After the 20th cycle, the capacity of the bare o-$LiMnO_2$ electrode decreased while that of the PVP-o-$LiMnO_2$ electrode continued to increase until the capacity remained steady at around 150 mAh g^{-1}. The appearance of voltage plateaus around 4 V can be attributed to the phase transformation of the orthorhombic phase to a spinel-like phase upon cycling [9,10], while the plateau around 2.9 V is ascribed to the pure orthorhombic phase. Voltage plateaus developed more clearly around 4 and 2.9 V, suggesting that Li intercalation occurred on different sites in the cycle-induced spinel $LiMn_2O_4$ [34]: the tetrahedral site when over 4 V and the octahedral site when over 3 V. As shown in the insets in Figure 7, the 4 V discharge plateau gradually divided into two subplateaus, demonstrating that the reordering of Li toward a cycle-induced spinel was in progress during the cycling.

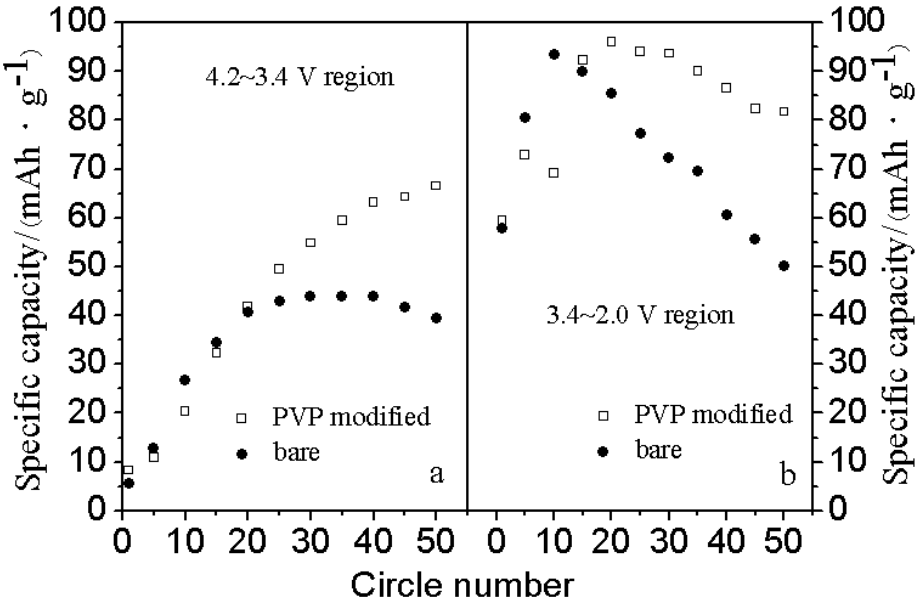

Figure 8. Cycling property of bare o-$LiMnO_2$ and PVP-o-$LiMnO_2$ at 0.5 C between the discharge voltage region of (a) 4.2 – 3.4 V and (b) 3.4 – 2.0 V

The capacities of the two plateaus plotted against the cycle number are shown in Figure 8. Using Figure 8, the discharge performances of the bare o-$LiMnO_2$ and PVP-o-$LiMnO_2$ in the different voltage regions can be more distinctly ascertained. In the 4.2 – 3.4 V discharge region (Figure 8a), the capacity of the bare o-$LiMnO_2$ decreased after the 40th cycle; at the 50th cycle, the capacity decreased to 39 mAh g^{-1} while the capacity of PVP-o-$LiMnO_2$ still increased. In the 3.4 – 2.0 V discharge region

(Figure 8b), the capacity of the bare o-$LiMnO_2$ decreased after 15 cycles whereas that of the PVP-o-$LiMnO_2$ decreased slowly after 30 cycles.

The improvement in the cycling property of PVP-o-$LiMnO_2$ can mainly be attributed to the stability of the spinel-like structure that arises from the PVP modification. As reported previously [23,35,36], the capacity fading of the o-$LiMnO_2$ materials occurred mainly in 3V region due to a collective Jahn-Teller distortion of the cycle-induced spinel-like phase. Additionally, the dissolution of manganese has been shown to lead to defective spinels [6,7,9] and hence poor cycling performance since, as mentioned above, the transformation of o-$LiMnO_2$ to a phase with a spinel-like structure occurs during cycling. Both the Jahn-Teller distortion and the dissolution of manganese are restrained by the modification of PVP to bare o-$LiMnO_2$. Lastly, the post oxygen treatment has also been shown to bring positive effects to the cyclability of PVP-o-$LiMnO_2$. Reddy et al. [30] found that the post oxygen treatment of PVP+PVA(Polyvinyl alcohol) -(MoO_3) played a significant role in activating the polymer as an electrochemical active species for lithium insertion.

4. CONCLUSIONS

The pure o-$LiMnO_2$ was synthesized by a solid-state reaction process using Mn_2O_3 and $LiOH{\cdot}H_2O$ as precursors, and then PVP was modified on the pure o-$LiMnO_2$ by a hydrothermal method to obtain PVP-o-$LiMnO_2$ cathode material. The results from this work showed that the PVP intercalated in o-$LiMnO_2$ and opened its interlayers, and that the C=O and C–N bonds in PVP bonded with the Mn atoms of the o-$LiMnO_2$. After the modification of PVP (about 3.7 wt.%), some fiber or stick typed crystals appeared in PVP-o-$LiMnO_2$ and the particles were smaller and narrower as compared to those in bare o-$LiMnO_2$. It was also demonstrated that the cyclability of PVP-o-$LiMnO_2$ cathode material was significantly improved due to the protection provided by the PVP of the spinel-like structure that formed on cycling. This study of the PVP modification of o-$LiMnO_2$ provides a facile way to improve the electrochemical performances of lithium-manganese-oxide compounds.

ACKNOWLEDGEMENTS
The authors wish to acknowledge the financial support for this work from the natural science foundation of Guangdong Province (Grant No. S2011010003416), the cooperation project in industry, education and research of Guangdong Province and Ministry of Education of P.R.China (Grant No. 2011B090400177), and the science and technology project of Huangpu District of Guangzhou.

References

1. J.W. Fergus， *J. Power Sources*, 195 (2010) 939.
2. C.H. Jiang, S.X. Dou, H.K. Liu, M. Ichihara and H.S. Zhou, *J. Power Sources*, 172 (2007) 410.
3. T. Takada, H. Hayakawa and E. Akiba, *J. Solid State Chem.*, 115(1995) 420.
4. Y.I. Jang, W.D. Moorehead and Y. Chiang, *Solid State Ionics*, 149(2002) 201.
5. Y.I. Jang andY.M. Chiang, *Solid State Ionics*, 130(2000)53.
6. Y.M. Chiang, H. Wang and Y.I. Jang, *Chem. Mater.*, 13 (2001) 53.

7. R.J. Gummow, D.C. Liles and M.M. Thackeray, *Mater. Res. Bull.*, 28(1993)1249.
8. I.J. Davidson, R.S. McMillan, J.J. Murray and J.E. Greedan, *J. Power Sources*, 54(1995) 232.
9. J.M. Kim and H.T. Chung, *J. Power Sources*, 115 (2003) 125.
10. S. H. Wu and M.T. Yu, *J. Power Sources*, 165 (2007) 660.
11. J.N. Reimers, E.W. Fuller, E. Rossen and J. R. Dahn, *J. Electrochem. Soc.*, 140 (1993) 3396.
12. S.T. Myung, S. Komaba and N. Kumagai, *Electrochim. Acta*, 47(2002) 3287.
13. H.M. Ji, G. Yang, X.W. Miao and A.Q. Hong, *Electrochim. Acta*, 55 (2010) 3392.
14. Z.P. Guo, K. Konstantinov, G.X. Wang, H.K. Liu, S.X. Dou, *J. Power Sources*, 119–121(2003)221.
15. L.J. Fu, H. Liu, C. Li, Y.P. Wu, E. Rahm, R. Holze and H.Q. Wu, *Prog. Mater. Sci.*, 50 (2005) 881.
16. C.H. Lu, H.C and Wang, *J. Eur. Ceram. Soc.*, 24(2004) 717.
17. A. D. Robertson, A. R. Armstrong, A. J. Fowkes and P. G. Bruce, *J. Mater. Chem.*, 11 (2001)113.
18. T.E. Quine, M.J. Duncan, A.R. Armstrong, A.R. Robertson and P.G. Bruce, *J. Mater. Chem.*, 10(2000) 2838.
19. Z.F. Huang, C.Z. Wang, X. Meng, D.P. Wang and G. Chen, *J. Solid State Chem.*, 179(2006)1602.
20. P. Suresh, A.K. Shukla and N. Munichandraiah, *J. Electrochem. Soc.*, 152 (2005)2273.
21. P. Suresh, A.K. Shukla and N. Munichandraiah, *Electrochem. Solid State Lett.*, 8(2005) 263.
22. Z. Su, Z.W. Lu, X.P. Gao, P.W. Shen, X.J. Liu and J.Q. Wang, *J. Power Sources*, 189 (2009) 411.
23. C. Li, H.P. Zhang, L.J. Fua, H. Liua, Y.P. Wu, E. Rahmb, R. Holze and H.Q. Wu, *Electrochim. Acta*, 51 (2006) 3872.
24. J. Cho, Y. Kim, T. Kim and B. Park, *J. Electrochem. Soc.*, 149(2002) A288.
25. J. Cho, Y. Kim, T. Kim and B. Park, *J. Electrochem. Soc.*, 149 (2002)A127.
26. G.G. Amatucci, A. Blyr, C. Sigala, P. Alfonse and J. M. Tarascon, *Solid State Ionics*, 104 (1997)13.
27. A. Du Pasquier, F. Orsini, A. S. Gozdz and J. M. Tarascon, *J. Power Sources*, 81–82(1999)607.
28. R.X. Yan, *Water-solubility Polymer*. Chemical Industry Press, Beijing(2001).
29. S.T. Myung, S. Komaba and N. Kumagai, *Solid State Ionics*, 150 (2002)199.
30. C.V.S. Reddy, Y.Y. Qi, W. Jin, Q.Y. Zhu, Z.R. Deng, W. Chen and S.I. Mho, *J. Solid State Electrochem.*, 11 (2007)1239.
31. Z.S. Peng, J. Ma, J. Di and Y.M. Chu, *J. Functional Mater.*, 30(1999) 379.
32. S. Sapra, J. Nanda, D.D. Sarma, F. Abed El-Al and G. Hodes, *Chem. Commun.*, 32(2001)2188.
33. S.H. Liu, X.F. Qian, J. Yin, X.D. Ma, J.Y. Yuan and Z.K. Zhu, *J. Phys. Chem. Solids*, 64(2003)455.
34. T. Ohzuku, M. Kitagawa and T. Hirai, *J. Electrochem. Soc.*, 137(1990) 769.
35. Y.I. Jang, B.Y. Huang, H.F. Wang, D.R. Sadoway and Y.M. Chiang, *J. Electrochem. Soc.*, 146 (1999) 3217.
36. S.T. Myung, S. Komaba and N. Kumagai, *Electrochim. Acta*, 47(2002)3287.